Optics and Laser Technology 103 (2018) 387–395

Contents lists available at ScienceDirect

Optics and Laser Technology

journal homepage: www.elsevier.com/locate/optlastec

Full length article

Fringe chasing by three-point spatial phase shifting for discrimination of the motion direction in the long-range homodyne laser Doppler vibrometry

Mohammad Hossein Daemi [a], Saifollah Rasouli [a,b,*]

[a] Department of Physics, Institute for Advanced Studies in Basic Sciences, Zanjan 45137-66731, Iran
[b] Optics Research Center, Institute for Advanced Studies in Basic Sciences, Zanjan 45137-66731, Iran

ARTICLE INFO

Article history:
Received 20 June 2017
Received in revised form 15 January 2018
Accepted 21 January 2018

Keywords:
Homodyne laser Doppler vibrometry
Three-points spatial phase shifting
Unwrapping tolerance value
Phase increments histogram

ABSTRACT

In this work, a three-point spatial phase shifting (SPS) method is implemented for chasing of the moving interference fringes in the homodyne laser Doppler vibrometry (HoLDV). By the use of SPS method, we remove disability of the HoLDV in the discrimination of the motion direction for long-range displacements. From the phase increments histogram, phase unwrapping tolerance value is selected, and adequacy of the data acquisition rate and required bandwidth limit are determined. Also in this paper, a detailed investigation on the effect of detectors positioning errors and influence of the Gaussian profile of the interfering beams on the measurements are presented. Performance of the method is verified by measuring a given harmonic vibration produced by a loudspeaker. Also, by the proposed method, vibration of mounting system of a disk laser gain medium is characterized.

1. Introduction

Vibrometry has a special significance in the science and engineering studies. One of the usual optical vibrometry methods is the Homodyne Laser Doppler Vibrometry (HoLDV) [1]. This method employs a two-beam interferometer in which one of the beams is reflected by the vibrating object. In this method, a fringe pattern with a large period is produced and a time-dependent intensity signal is accumulated by a point intensity detector. By changing optical path difference of the interferometer's arms in an interval larger than a quarter of the interfering beams' wavelength, the absolute values of the detectable minimum and maximum intensities are determined. At the equilibrium position of the object, the optical path difference of the interferometer's arms is tuned in such a way the detected signal is the mean value of the absolute minimum and maximum intensities. In this point, known as the quadrature point, the intensity variation due to the object motion is maximum. For small enough values of the object displacements, and at the vicinity of the quadrature point, the response function of the system, defined as the detected intensity against displacement, is linear. For the vibrations with very small values of the amplitudes compared to the interfering beams' wavelength, the intensity signal yields all of the necessary data for the reconstruction of the motion.

In the conventional HoLDV, by increasing the displacement value, the response function of the system gets a sinusoidal form. For a given motion with a maximum displacement larger than a quarter of the wavelength of the interfering beams, after the moment that the detected signal experiences one of the extremum values, determination of the displacement direction is not possible. In other words, in this case, the signal trend does not reflect the direction of the motion and it leads to an ambiguity in the motion reconstruction.

A well-known method for removing the mentioned ambiguity is the use of the heterodyne LDV technique [2]. In this technique a fixed high frequency-shift is applied between the interfering beams, with an order of tens of MHz. Therefore, a fixed-frequency beating is produced even with a non-moving object. Displacement of the object, changes the frequency of the beating. The direction of the displacement is discriminated by the sign of beating frequency change. In this technique, as the beating rates are very high, analog frequency demodulation techniques should be used to extract the vibration characteristics. Another method named pseudo-heterodyne was also used to produce high frequency beating by changing the wavelength of the reference beam [3,4], or by a gradually increasing/decreasing of the reference arm's

* Corresponding author at: Department of Physics, Institute for Advanced Studies in Basic Sciences (IASBS), No. 444, Prof. Yousef Sobouti Blvd., P. O. Box 45195-1159, Zanjan 45137-66731, Iran.
E-mail address: rasouli@iasbs.ac.ir (S. Rasouli).

https://doi.org/10.1016/j.optlastec.2018.01.056
0030-3992/

length [5]. Comparing to the HoLDV, implementation of these methods needs more complicated equipment.

It is worth mentioning that by employing quadrature fringe detection method in HoLDV setup, it is possible to overcome to the above-mentioned disability of the HoLDV for discrimination of the motion direction [6–8]. This method can be utilized by using a double polarized laser, a proper combination of polarization beam splitters and quarter-wave plates, and an additional detector in the HoLDV setup. Homodyne interferometry with quadrature fringe detection provides two quadrature signals from the same output source, where their values retrieve the direction of motion and instantaneous position of the vibrating object. The quadrature detection of a Doppler signal has also drawbacks and needs additional hardware, such as a fully stable double polarized laser.

In this work, by the aid of fringe chasing we present a method to determine the direction of motion by HoLDV setup. In comparing with the quadrature fringe detection method, our HoLDV setup is simple and there is no need to the fully stable double polarized laser beam and other additional hardware. For the fringe chasing, we implement a three-point spatial phase shifting (SPS) method and we measure instantaneously the phase of fringe pattern. By this kind of homodyne detection, large-amplitude motions can be easily investigated. In addition, we will show that by the aid of the three-point fringe chasing method, despite of the conventional HoLDV, it is not necessary to tune the system on the quadrature point.

It should be noted that the chasing of the fringes motion can be done by inspection of the successive frames of a movie that is taken from the fringe pattern during the object vibration. Also this can be done by a linear array sensor. In these cases, the sampling rate is decreased due to the low frame/line rates of the recording systems in comparing to the case of three point-detectors. In addition, for high frame/line rates typically over than a 10 kHz rate, these instruments are expensive, volume of the data is huge, and the data transferring processes are time-consuming. On the other hand, for an interference pattern with a sinusoidal profile and known spatial period, knowing the intensities of only three points over a period is enough to calculate the pattern phase. Therefore, apparently the additional data supplied by the 2D or linear array sensors limit the sampling rate. The use of three-point detection remarkably increases sampling rate with respect to the mentioned sensors. For this reason, the proposed three point-detector can be easily extended to the ultrasound regime.

It worth mentioning that, already the N-point SPS method has been used for the detection and compensation of the environmental vibrational noise but the vibration characteristics has not been investigated [9]. Also, in two other works, two different arrangements of the two-point SPS method [10,11], were proposed for the reconstruction of the motion. These arrangements can be only applied when the visibility of fringes is very close to one. Therefore, this condition is not always satisfied. In another work, a similar formulation has also been used to analyze the 2D vibrational modes and the resonant frequencies of a flat speaker [12], where the amplitude of the vibration has been measured, but the temporal behavior has not been recorded.

As the measured phase obtained by implementing SPS method on a HoLDV has a wrapped form, using the phase increments histogram, we present a simple way for selection of the phase unwrapping "tolerance value". Also, the adequacy of the data acquisition rate and required bandwidth limit are determined from the resulted phase increments histogram of the motion. As the positioning of the detectors at the desired positions accompanies with error, in this work we also present an investigation on the effect of detectors positioning errors on the measurements. Also, the influence of the Gaussian profile of the interfering beams on the results is investigated.

Reliability of the proposed method is examined by simulations of a motion with a constant velocity and a harmonic vibration. Finally, we use the method for detection of vibrations of the mechanical mounting of a thin disk laser gain medium. In the following, formulation of the SPS method in a general form is presented.

2. Homodyne LDV

The HoLDV is based on the two-beam interferometry where one of the beams carries the vibrational information of a single point on the vibrating object via Doppler shift in its wavelength. For a better understanding of the results of the present work, here a brief review on the HoLDV is presented.

For a Michelson type interferometer, the normalized instantaneous intensity is of the form

$$I(t) = 1 + V\cos(2k\Delta L(t)), \tag{1}$$

where $k = 2\pi/\lambda$, is the wavenumber of the reference or probe beam, and $\Delta L(t)$ is the optical path difference (OPD) of the interferometer arms. V is a parameter that specifies contrast of the temporal signal. The OPD can be separated into two parts; the mean OPD, ΔL_0 and a time-varying part corresponding to the vibration, $X(t)$.

For a harmonic vibration $X(t) = A\cos(\Omega t)$ with an angular frequency of Ω and an amplitude of A, the signal of Eq. (1), can be written as

$$I(t) = 1 + V\cos\phi\cos[2kA\cos(\Omega t)] - V\sin\phi\sin[2kA\cos(\Omega t)], \tag{2}$$

where $\phi = 2k\Delta L_0$ is the phase difference between the beams at the equilibrium position of the object. Using the real-valued forms of Jacobi–Anger identities [13]

$$\begin{aligned}\cos(x\cos\theta) &= J_0(x) + 2\sum_{n=1}^{\infty}(-1)^n J_{2n}(x)\cos(2n\theta),\\ \sin(x\cos\theta) &= -2\sum_{n=1}^{\infty}(-1)^n J_{2n-1}(x)\cos[(2n-1)\theta],\end{aligned} \tag{3}$$

where $J_n(x)$ is the first kind Bessel function of order n, Eq. (2) can be rewritten as

$$\begin{aligned}I(t) = 1 &+ V\left\{J_0(2kA) + 2\sum_{n=1}^{\infty}(-1)^n J_{2n}(2kA)\cos(2n\Omega t)\right\}\cos\phi\\ &- V\left\{2\sum_{n=1}^{\infty}(-1)^n J_{2n-1}(2kA)\cos[(2n-1)\Omega t]\right\}\sin\phi.\end{aligned} \tag{4}$$

Eq. (4) yields the coefficients of the Fourier series expansion of the HoLDV signal. This means that, despite of the pure harmonic oscillation of the object at a single frequency, there are many higher harmonics in the spectrum of the signal. Higher the amplitude, higher the order of Bessel functions with a noticeable contribution. The contributions of the odd or even harmonics are governed by the parameter ϕ. For a special case of $\phi = m\pi$ with m an integer number, the main vibration frequency will be absent in the spectrum!

At the vicinity of the quadrature points where $\phi = m\pi + \pi/2$ (depicted by a dark dot in the Fig. 1), the sensitivity of the detected intensity to the displacement of the vibrating object is maximum. For an enough small vibration amplitude, the response function of the LDV system will be approximately linear. So, this technique is mostly used in the detection of the ultrasonic waves that the amplitude of vibration is generally limited to around few tens of nanometer or less [14].

In Fig. 1 a typical sinusoidal vibration of an object and its simulated HoLDV signals are plotted. According to the figure, each of two adjacent regions where the intensity variation is slow,

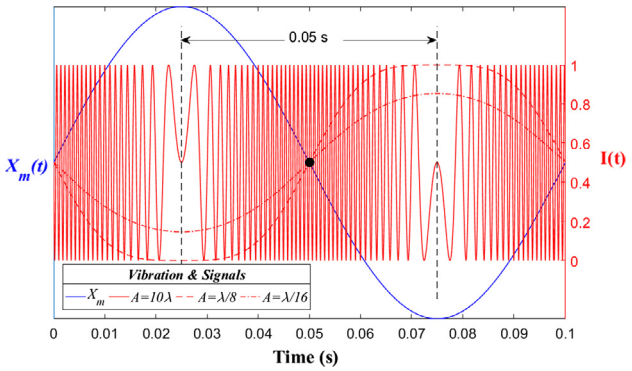

Fig. 1. A typical sinusoidal vibration of an object with a frequency of $f = 10$ Hz (blue) and corresponding simulated HoLDV normalized signals (red) for vibration amplitudes of 10λ (solid), $\lambda/8$ (dashed), and $\lambda/16$ (dashed-dotted). (For interpretation of the references to color in this figure legend, the reader is referred to the web version of this article.)

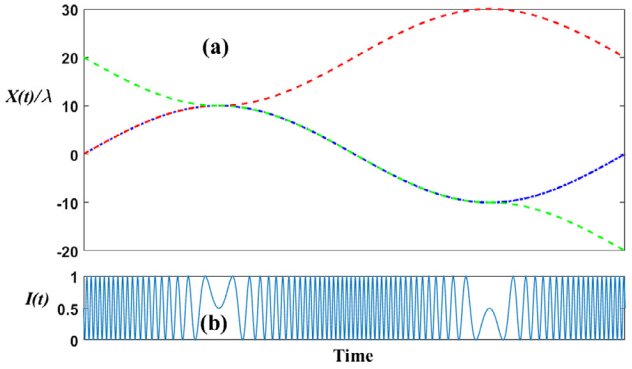

Fig. 2. (a) Illustration of three typical long-range motions, and (b) their corresponding identical HoLDV signal. Plot in (b) shows that the signal is insensitive to the change of the direction of motion.

depicted by two vertical dashed lines, are correspond to two opposite extremums of the vibration, so the time interval between them is a half of the vibration period. There are 40 fringes within the time interval, that means $40 \times \lambda/2 = 20\lambda$ peak-to-valley (PV) of the vibration.

For a harmonic vibration with a large value of amplitude, the frequency and amplitude of the vibration can be extracted by fringe counting of the signal, Fig. 1. But, for non-harmonic and random vibrations with large fluctuations, as the motion is not predictable and because of the non-monotonic nature of the cosine function in Eq. (1), the interpretation of the detected signal is not straightforward. In Fig. 2, the degeneracy of the HoLDV signal for three different motions are illustrated, where all of the three depicted motion waveforms in (a) produce a same signal as shown in (b).

3. Fringe chasing

We consider that the light source sends a plane monochromatic wave into a Michelson's interferometer, and on the observation plane the propagation directions of the reflected beams from the mirrors get an angle θ with each other. Two reflected beams interfere and the resulted intensity pattern can be written as

$$I(x,t) = I_1 + I_2 + 2\sqrt{I_1 I_2}\cos\left[(2\bar{k})x\sin\left(\frac{\theta}{2}\right) - \Delta\omega t\right], \quad (5)$$

where I_1 and I_2 are the intensity of the beams, $\bar{k} = (k_1 + k_2)/2$ is the average of the wave-numbers k_1 and k_2 of the interfering beams, $\Delta\omega = \omega_2 - \omega_1$ is the angular frequency difference of the beams caused by the motion of the object, and x shows the direction perpendicular to the bisector of the beams propagation directions. The period of the resulted fringes in the x-direction, Λ, and time-dependent phase, $\Phi(t)$, are

$$\Lambda = \frac{\bar{\lambda}}{2\sin(\theta/2)}, \quad \Phi(t) = \Delta\omega t = 2\pi\Delta\nu t, \quad (6)$$

respectively, where $\bar{\lambda} = 2\pi/k$. The time dependency of the phase in Eq. (5) means that the pattern is moving with a velocity $u_f = \Delta\omega/2\bar{k}\sin(\theta/2)$. With u_m as the velocity of the moving object, the Doppler shift is $\Delta\omega = \omega_0 2u_m/c$. Considering $u_f = dX_f/dt$ and $u_m = dX_m/dt$, where X_f is the position of an arbitrary point of the fringe pattern along the x -axis, and X_m is the out-of-plane displacement of the vibrating object, after a time integration of u_m we have

$$X_m = \sin(\theta/2)X_f + X_0. \quad (7)$$

This is a linear function that relates the location of a special point in fringe pattern to the out-of-plane position of the object. The value of X_0 depends on the position of the selected point on the fringe pattern. Here only the relative displacement of the vibrating object is desired, then X_0 can be ignored. Eq. (7) shows the linear dependence of the fringe position on the object position with the magnification factor of $1/\sin(\theta/2)$.

There is two distinct ways for chasing the fringe pattern; to measure the displacement of a specific point of the fringe pattern with respect to a fixed point in the lab frame that we call it **direct chasing**, or to measure the phase of fringe pattern at a fixed point in the lab frame. We name the latter one as the **indirect chasing**. In the indirect-chasing method, by the measurement of the phase $\Phi(t)$ of the sinusoidal fringe pattern at a given point in the lab frame we calculate X_f by

$$X_f = \frac{\Phi}{2\pi}\Lambda. \quad (8)$$

In the next section, determination of the time dependency of the fringe's phase, $\Phi(t)$, at a given point by SPS method, and consequently the fringe displacement is presented.

4. Spatial phase shifting

There are a variety of N-Point ($N \geq 3$) algorithms that can be used in the detection of the phase of a fringe pattern having a sinusoidal profile [15]. In this work by knowing value of the spatial period of the fringe pattern, Λ, we use the 120° three-point method. In practice we install the detectors at equal distances as possible as, then by tilting the reference mirror of the interferometer the desired Λ is achieved. Tuning of the Λ and positioning of the detectors accompany with some errors which lead to an error in the reconstructed waveform of the motion.

It worth noting that to overcome the error of matching the fringe pattern period to the distances between the detectors, one can use Carré algorithm with 4 detectors [16]. In the Carré algorithm, the error on the reconstructed motion due to the unequal spacing of the detectors is still present.

Because of some practical limitations, such as large dimensions of the detectors and limited lateral size of the interfering beams, it is preferred to use less number of detectors. Therefore, for easier installing and also reducing the volume of the data, here we use 120° three-point algorithm. Furthermore, the acceptable range of the tuning errors will be determined by simulation of the effect of these errors on the reconstructed motion.

Now we present the three-point SPS algorithm for the fringe phase calculation. One can rewrite Eq. (5) in the following general form:

$$I(x,t) = a + b\cos\left(\frac{2\pi}{\Lambda}x + \Phi(t)\right), \tag{9}$$

where a and b determine the visibility of the fringe pattern. For determining unknown $\Phi(t)$ of a given fringe pattern, as there are two other unknown parameters a and b we need to know the intensity values at least for three points. Typical two-beam interference pattern and locations of the three detectors are shown in Fig. 3.

If Λ is divided into N equal sections (three sections as in Fig. 3), from Eq. (9)the intensity at the start point of the nth section can be written as

$$I_n = a + b\cos\left(\frac{2\pi}{\Lambda}x_n\right)\cos(\Phi) - b\sin\left(\frac{2\pi}{\Lambda}x_n\right)\sin(\Phi), \tag{10}$$

where it is assumed that the first section begins from the maximum intensity on the pattern. Multiplying both sides by $\cos(2\pi x_n/\Lambda)$ and then by an average over all possible n values we have

$$\frac{1}{N}\sum_{n=1}^{N} I_n\cos\left(\frac{2\pi}{\Lambda}x_n\right) = \frac{a}{N}\sum_{n=1}^{N}\cos\left(\frac{2\pi}{\Lambda}x_n\right) + \frac{b}{N}\cos(\Phi)\sum_{n=1}^{N}\cos^2\left(\frac{2\pi}{\Lambda}x_n\right) - \frac{b}{N}\sin(\Phi)\sum_{n=1}^{n}\sin\left(\frac{2\pi}{\Lambda}x_n\right)\cos\left(\frac{2\pi}{\Lambda}x_n\right). \tag{11}$$

By considering the fact that the *odd* sentences of sine and cosine functions over a full period is zero, the relation will be

$$\sum_{n=1}^{N} I_n\cos\left(\frac{2\pi}{\Lambda}x_n\right) = \frac{b}{2}\cos(\Phi). \tag{12}$$

Similarly, after multiplying by $\sin(2\pi x_n/\Lambda)$ and then averaging we have

$$\sum_{n=1}^{N} I_n\sin\left(\frac{2\pi}{\Lambda}x_n\right) = -\frac{b}{2}\sin(\Phi). \tag{13}$$

Dividing both sides of last two equations, the phase of the fringe pattern at a given time is determined by

$$\Phi = \tan^{-1}\left[-\frac{\sum_{n=1}^{N} I_n\sin\left(\frac{2\pi}{\Lambda}x_n\right)}{\sum_{n=1}^{N} I_n\cos\left(\frac{2\pi}{\Lambda}x_n\right)}\right]. \tag{14}$$

In the case of three-point SPS, the locations are $x_1 = 0, x_2 = \Lambda/3$, and $x_3 = 2\Lambda/3$, respectively, so the resulted phase of the fringe pattern will be

$$\Phi_{3-point} = \tan^{-1}\left[-\frac{I_1\sin(0) + I_2\sin\left(\frac{2\pi}{3}\right) + I_3\sin\left(\frac{4\pi}{3}\right)}{I_1\cos(0) + I_2\cos\left(\frac{2\pi}{3}\right) + I_3\cos\left(\frac{4\pi}{3}\right)}\right] = \tan^{-1}\left[\sqrt{3}\frac{I_3 - I_2}{2I_1 - (I_2 + I_3)}\right]. \tag{15}$$

For 4-point phase shift, similarly we have

$$\Phi_{4-point} = \tan^{-1}\left[\frac{-I_2 + I_4}{I_1 - I_3}\right]. \tag{16}$$

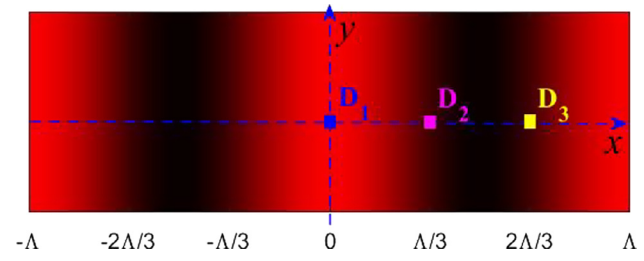

Fig. 3. Typical two-beam interference pattern and detectors' relative positions for the implementation of three-point SPS method.

As is apparent, removing of the above-mentioned ambiguity in the motion direction determination, is due to the monotonic nature of the arctangent function of Eq. (14).

Here, the lateral size of the field of view is larger than to $2\Lambda/3$ to cover all detectors. For a displacement of the object larger than $\lambda/2$, one full period of fringe pattern moves away from the field of view. In such a case, a π jump (up or down depending on the direction of the motion) appears on the calculated phase. These jumps should be "unwrapped" to yield the actual phase.

5. Simulation of two simple motions

In following, simulation of two simple motions is presented.

5.1. A motion with constant velocity

For a typical linear motion of an object with a constant velocity, according to Eq. (1), each detector records a cosine signal with a DC level (Fig. 4). The frequency of the signal is proportional to the velocity of the object. All detectors experience same signal, but with a $2\pi/3$ phase delay between the successive detectors. The resulted phase is straight line versus time, that experiences wraps at $\Phi = \pm(2m+1)\pi/2$. Differentiating Eq. (8) and substituting relevant parameters, shows that the slope of $\Phi(t)$ is a constant value

$$\dot{\Phi} = \frac{2\pi}{\Lambda}\dot{X}_f = \frac{2\pi}{\Lambda}\frac{1}{\sin(\theta/2)}u_m = \frac{4\pi}{\lambda}u_m \doteq \alpha = \text{constant}. \tag{17}$$

This relation also discloses the dependency of the rate of the pattern phase change to the probe beam wavelength. According to Eq. (17), smaller wavelength leads to more rapid phase change, although as shown by Eq. (7), the fringe motion velocity is *independent* of the probe beam wavelength. By unwrapping the phase depicted in Fig. 4, the expected linear curve with a constant slope angle is obtained. In Fig. 4, the constant speed of the linear motion is 1 mm/s and the probe beam wavelength is 632.8nm. Phase drops occur at times that the denominator of Eq. (15) is zero and then $\Phi = \pm(2m+1)\pi/2$. Temporal contrast of the signals is considered to be $V = 1$ and sampling rate is $f_s = 1$ MS/s.

From Eq. (17), for equal and constant sampling time interval of the signals ($\Delta t = 1/f_s = \text{const.}$), one can expect that for the velocity of $\pm u_m$, the phase increment at each time step is $\Delta\Phi_1^{\pm} = \dot{\Phi}\Delta t = \pm 4\pi u_m/\lambda f_s$, except in the vicinity of the discontinuities, where the phase increment is $\Delta\Phi_2^{\mp} \approx \mp\pi$. In fact, the phase increments are populated around two distinct values of $\Delta\Phi_1^{\pm}$ and $\Delta\Phi_2^{\mp}$, (Fig. 5). Useful information about the motion can also be extracted from the histogram of these phase increments. For the

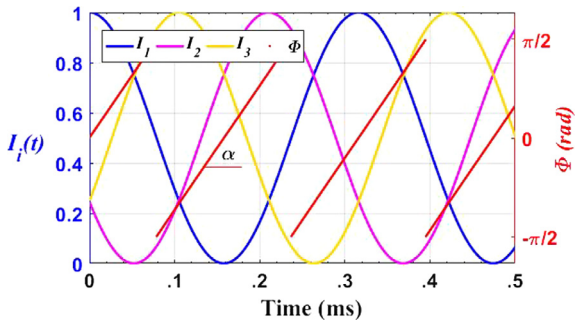

Fig. 4. Simulated three-point SPS intensity signals (Blue, pink and yellow) for a linear motion with a constant velocity of $u_m = 1$ mm/s and corresponding calculated phase of the moving pattern (red). The probe beam wavelength is $\lambda = 632.8$ nm. Phase delay between two adjacent detectors is $2\pi/3$ rad. (For interpretation of the references to color in this figure legend, the reader is referred to the web version of this article.)

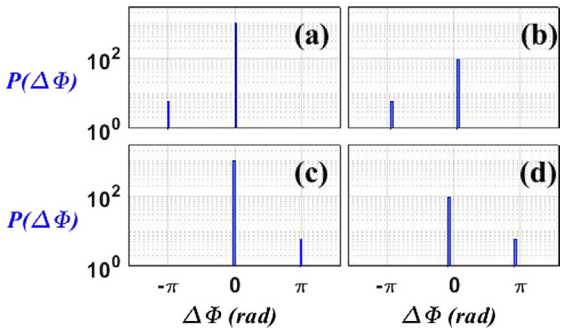

Fig. 5. Phase increment histograms for a linear motion with a constant velocity and probe beam wavelength of $\lambda = 632.8$ nm. Velocity u_m and sampling rate f_S are: (a) 1 mm/s and 1.0 MS/s, (b) 1 mm/s and 0.1 MS/s, (c) −1 mm/s and 1.0 MS/s, and (d) −1 mm/s and 0.1 MS/s, respectively.

data of Fig. 4, corresponding histograms in 1ms time duration, for two different sampling rates, and two opposite directions of motion are shown in Fig. 5. Population of $\Delta\Phi_1$ depends on the data acquisition rate where its value is 93 for 0.1 MS/s and is 993 for 1.0 MS/s, at the time, the population of $\Delta\Phi_2$ is 6 for both of the sampling rates. $\Delta\Phi_2$ corresponds to the net number of half-fringes move away from the field of view. This means that more than 6 half-periods of interference pattern (and less than 7), moved away from the field of view of the three point-detectors. This is equivalent to the well-known fringe counting method. For more precise estimation of the displacement, the value and population of $\Delta\Phi_1$ should also be considered. After unwrapping process, the populations of $\Delta\Phi_2^{\mp}$ will be added to the $\Delta\Phi_1^{\pm}$ and the phase increments will be equal in all time steps.

5.2. Harmonic vibration

In the harmonic vibration of the object, especially for large values of the amplitude, chirped sinusoidal signals are detected as shown in Fig. 1. During a cycle of vibration, two chirped periods appear. Each chirped period contains both of positive and negative chirps with a mirror symmetry on the signal. Number of intensity oscillations in a chirped period depends on the amplitude of the vibration. Despite of the previous example where the calculated phase was straight lines between the jumps, here it is expected that the calculated phase to be a piece of a cosine function between successive phase jumps, which after unwrapping, reproduces the harmonic motion. In Fig. 6 detection of a typical harmonic motion

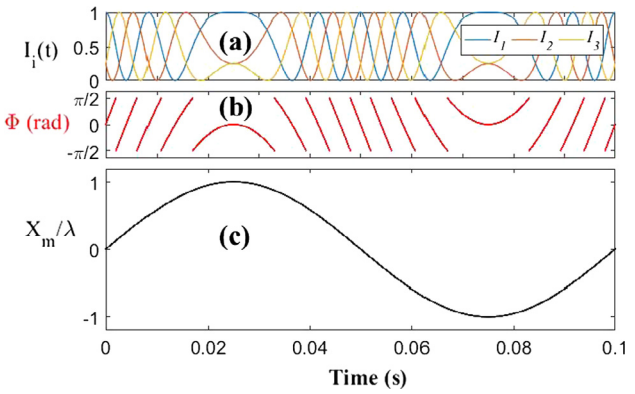

Fig. 6. (a) Illustration of the chirped signals corresponding to a harmonic vibration of the object with an amplitude equals to the probe beam wavelength and frequency of 10 Hz, (b) calculated phase, and (c) the reconstructed displacement of the object. In the calculations a sampling rate of 1.0 MS/s is considered.

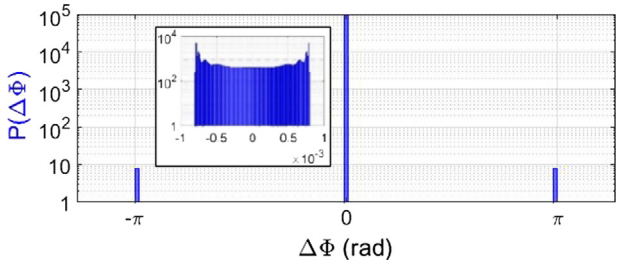

Fig. 7. Phase increments histogram for a harmonic motion of Fig. 6. The inset shows the central populated region in an enlarged view.

by a three-point SPS is illustrated. Like the case of linear motion, phase discontinuities appear at the points where Eq. (15) diverges.

Here again the object displacement can be determined from the histogram of $\Delta\Phi$ (Fig. 7). Because of bi-directionality of the motion, there are two populated regions in the vicinities of $\Delta\Phi_2^{+} = +\pi$ and $\Delta\Phi_2^{-} = -\pi$, and two highly populated regions $\Delta\Phi_1^{+}$ and $\Delta\Phi_1^{-}$ located very close to each other, almost symmetrically around zero (the inset of the Fig. 7). Equality of the populations around $\pm\pi$ values reflects that the net displacement is almost zero. More precise value of the displacement can be determined by considering the contributions of the $\Delta\Phi_1^{\pm}$. The population of 8 for $\Delta\Phi_2^{\pm}$ indicates that there are 8/2 = 4 fringes between two extremums, so the object displacement between the extremums is $4 \times \lambda/2 = 2\lambda$, and then, the amplitude of the vibration is $A = \lambda$.

Any unbalanced populations for the positive and negative areas, can be interpreted as a net displacement of the object during the sampling time interval.

In both of examples stated in this section, as the sampling rates were high enough, the phase increments histograms have wide unpopulated regions between the central and side lobes. The unwrapping tolerance value should be selected within these un-populated regions. This requirement will be more important in actual cases with limited acquisition rate.

6. Implementation issues

In this section, some implementation issues consisting of the detectors positioning errors, effect of the Gaussian profile of the interfering beams, and sampling rate on the measurements are presented.

6.1. Effect of positioning errors

Here we investigate the effect of the detectors positioning errors on the results. As a given motion of the object can often be decomposed to Fourier components; in the following we consider a harmonic motion in three-point SPS method.

Any error in the positioning of the detectors causes erroneous relative phase delays. In this case, the reconstructed waveform of the motion will be *distorted*. Meanwhile, because of the repetitive nature of the process, the repetition rate of the reconstructed waveform is equal to the vibration frequency. We assume that the detector D_1 is located at the origin (Fig. 3), therefore in the calculation of the distortion, it is enough to consider only positioning errors of D_2 and D_3 detectors. This error analysis also will cover the fringe period tuning error. A typical waveform distortion and related spectrum for non-accurate positioning of D_2 is illustrated in Fig. 8. Reconstructed waveform distortion has an additive chirped oscillation term (red[1] plot of Fig. 8a). Due to the chirped

[1] For interpretation of color in Fig. 8, the reader is referred to the web version of this article.

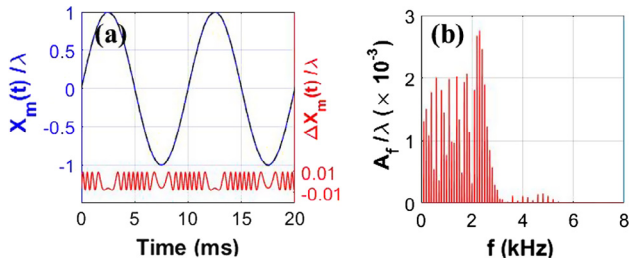

Fig. 8. A Typical sinusoidal motion with a distortion caused by a given error on the position of D_2, $\Delta_{x2} = 0.15\Lambda$ and (b) spectrum of the distortion. Here, misplacement of D_2 is $\Lambda/6$, THD = 8.55×10^{-4}, and PV/A ~ 1.7%. In (a) data during 2 periods and in (b) corresponding spectrum of 100 periods of the object vibration are shown, respectively.

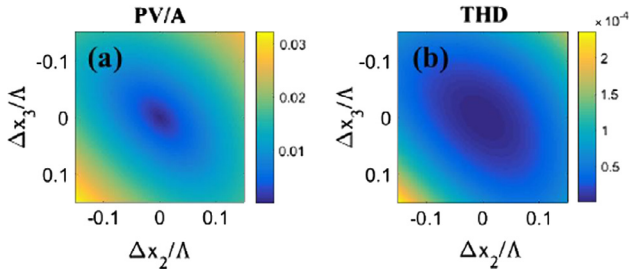

Fig. 9. Effect of the detectors positioning error (in the range of $\pm 0.15\Lambda$) on PV/A (a) and THD (b) parameters.

nature of the distortion, *higher harmonics* will appear in its spectrum (Fig. 8b). Any change on the magnitude of the positioning error, causes changes on the chirping and corresponding spectrum.

To quantify the effect of the errors on the of reconstructed waveform distortion, we express the amount of distortion by two parameters; one is the ratio of the Peak to Valley of the distortion to the amplitude of vibration (PV/A) and another one is the Total Harmonic Distortion (THD) parameter. Here, THD is defined as the ratio of the power of all higher harmonics to the power of the measured waveform [17]. According to the Parseval's theorem [13], one can calculate the sum of the square of the distortion data, instead of integrating over the spectrum of the data, so

$$\mathrm{THD} = \sum_i (X_{rec,i} - X_{obj,i})^2 \Big/ \sum_i X_{rec,i}^2, \tag{18}$$

where $X_{obj,i}$ and $X_{rec,i}$ are the actual and reconstructed values of the position at ith sample. Summations are done over all of the samples during one complete cycle of the vibration. Because of the repetitive nature of the distortion, considering more cycles will not change the result. In Fig. 9, the calculated values of PV/A and THD for different values of D_2 and D_3 positioning errors are shown. For experimentally achievable values of Δx_2, $\Delta x_3 = \pm\Lambda/10$, according to Fig. 9, PV/A = 0.02, and THD = 10^{-4}, which means that the method is very tolerant to the detectors positioning errors.

6.2. Influence of the Gaussian profile of the beams

The finite dimension of the interfering beams and their commonly Gaussian intensity profiles affect the desired sinusoidal

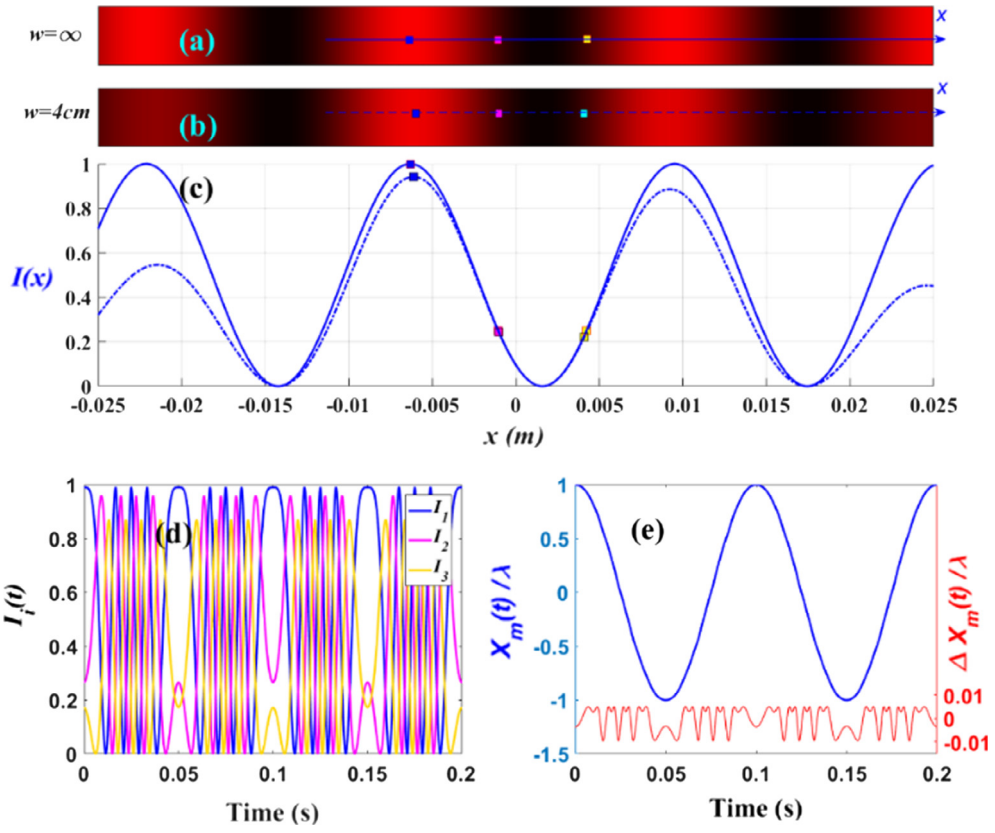

Fig. 10. Fringe patterns produced by interfering of two (a) plane beams with constant profiles, (b) Gaussian beams with a same 4 cm waists, and (c) their corresponding intensity profiles. (d) Three detectors' data during two periods of the vibration for a case of finite beams and (e) the reconstructed waveform with the unwanted distortion is shown by the red plot.

intensity profile of the resulting fringes. This means that the peak intensity and even fringe period are not constant everywhere on the pattern. For a given value of the probe beam waist $w = 4$ cm, the effect of this phenomenon is illustrated in Fig. 10 and compared with the ideal situation. Here $A = 1\lambda$ and the ratio of fringe spacing to the beam waist is $\Lambda/w \sim 0.4$. Normalized peak to valley of the distortion is calculated about PV/A $\sim 1.5\%$. If the detectors are installed more distant from the pattern center, the distortion will be larger.

6.3. Sampling rate remarks

In the simulated examples of Section 5, due to large number of samples in each of the signals, the motions were reconstructed with negligible errors. In practice due to the instrumental limits, data acquisition rate is limited, that may affect the accuracy of the waveform reconstruction. We know that for the case of an accelerated motion, there are a large number of higher harmonics in the Fourier spectrum of the corresponding signal. Let us estimate the reconstruction precision by considering the maximum possible sampling rate of the recording system and data storage capacity. Minimum permissible sampling rate is governed by the maximum velocity of the object. In a harmonic vibration, maximum value of the velocity is $u_{max} = A\Omega$, so the maximum beating frequency is $f_{b,max} = 2A\Omega/\lambda$. As the Nyquist's frequency is $f_N = 2f_{b,max}$, the sampling rate should be $f_s \geq 4A\Omega/\lambda$. In Fig. 11, histogram of the phase increments for different values of f_s are shown. The vibration amplitude and frequency are $A = 10\lambda$ and $f = 100$ Hz, respectively, so with $\lambda = 632.8$ nm the Nyquist's frequency is $f_N = 25$ kHz. For low sampling rates the populated areas will be broadened and the width of the un-populated areas will be decreased. In an extreme case of the fully-populated histogram, the reconstruction is impossible.

7. Experimental works

We have verified the proposed method by measuring the vibration of a loudspeaker which was driven with a harmonic function generator.

In Fig. 12 a schematic diagram of the experimental setup is shown. A Michelson interferometer is installed in which the object beam is reflected from a mirror-like part of the loudspeaker. A He-Ne laser with a wavelength of $\lambda = 632.8$ nm feeds the interferometer. Interference pattern of the reference and object beams is magnified and guided, by the aid of a lens and three steering mirrors onto three point-detectors (reversely biased DET10A, Thorlabs). Spatial period of the vertical fringe pattern is tuned by tilting mirror M1 to be about 5 cm at the detectors. The detectors are installed in which their phase delays were $2\pi/3$ rad.

The bandwidth of the measuring system should be high enough in comparison to the highest repetition rate of the chirped signals. The magnitude of the termination resistor R_T, which converts the current signal of a detector to a voltage signal, determines the signal strength of the signal. On the other hand the R_T value governs

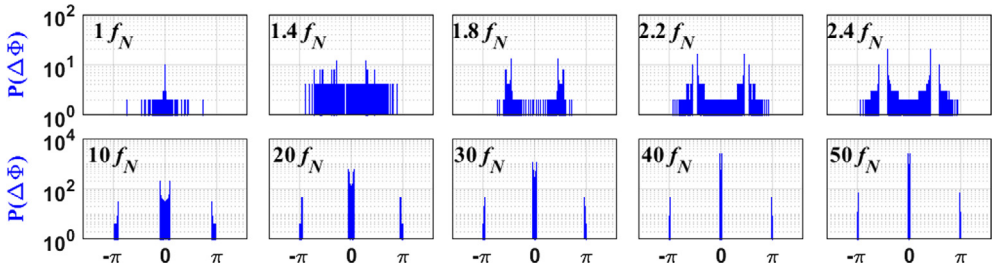

Fig. 11. The histograms of the phase increments at different values of sampling rate, from $1f_N$ to $50f_N$. The vibration amplitude and frequency respectively are $A = 10\lambda$, $f = 100$ Hz, and with $\lambda = 632.8$ nm, $f_N = 25$ kHz.

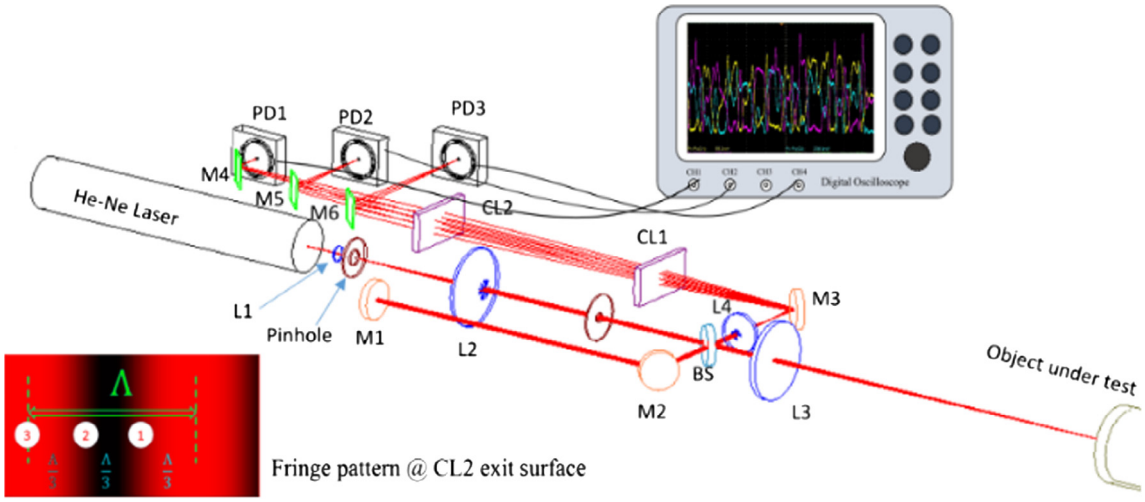

Fig. 12. Optical setup for the implementation of the three-point SPS method. Two lenses **L1** and **L2** with the pin-hole are used as spatial filter to produce plane wave. The lens L3 is for focusing the beam on the vibrating surface of the object under test. The lens L4 is for expansion of the fringe pattern. BS is a beam splitter. M1–M6 are HR flat mirrors, which the last 3 mirrors can be used -by angle adjustment- to phase shift tuning. Tip-tilt adjustment of M1 is employed for making linear vertical fringe pattern with a suitable fringe spacing. CL1 and CL2 are cylindrical lenses for focusing the pattern in the vertical direction to attain higher intensity contrast. The inset shows resulted linear fringe pattern at the exit plane of the CL2. PD1, PD2 and PD3 are photodiodes that are measuring the intensity at the points 1, 2, and 3 depicted in the inset figure.

the transmission line bandwidth via the well-known relation, $f_{BW} = (2\pi R_T C_j)^{-1}$ with $C_j \sim 6$ pF [18] as the junction capacitance of employed photodiodes.

In Fig. 13 the results of a typical measurement of the loudspeaker vibration are presented. The amplitude derived from the proposed fringe chasing method is 49.66 μm, which is in good agreement with the fringe counting result. We counted about 316 complete fringes beating between two successive large-period regions of the signal, which corresponds to a $316 \times \lambda/2 = 99.98$ μm distance between two extremums of the vibration or 49.99 μm of the amplitude. Data acquisition rate was 25 MS/s. The transmission bandwidth was 2.68 MHz using a 10 kΩ termination resistor parallel with the oscilloscope input impedance (1 MΩ). In (a) and (b) detected signals and calculated fringe phase in a time interval of 0.01 s are shown. In (c) and (d) the same parameters are shown for a smaller time interval of 2 ms respectively. The histogram of the phase increments is shown in (e). Existence of un-occupied regions in the histogram, guarantees a precise reconstruction of the motion, (f).

In Fig. 14, the results of the same experiment of Fig. 13 with a termination resistor $R_T = 100\Omega$ are shown. Here, although the bandwidth is a very high value of 0.265 GHz, the signals are very weak and comparable to the noise. So despite of the very high data acquisition rate, the calculated phase values at each step of data acquisition period is randomly distributed (b). The histogram (c) has also no un-occupied region.

As a real life application of the proposed method, vibrational characteristics of the mounted gain medium of a thin disk laser which can be impinged with the cooling water flow was measured. The disk is mounted on a robust metal mount. Fig. 15 shows the system response to a mechanical impulse in the absence of the water flow. The impulse was exerted on different points of the system and the out-of-plane vibration of the disk was measured. Data acquisition rate and time interval were 50 kS/s and 10 s, respectively. As it appears from the histogram of the phase increments, (c), there are population-free regions that guarantee validity of the reconstruction. (d) and (f) show the damping of the oscillation for a 10 s 4 s time intervals, respectively. From the fast Fourier transform of the motion waveform (e), a value of ~ 30 Hz for the natural vibration frequency of the system is obtained. The damping coefficient of the system can also be

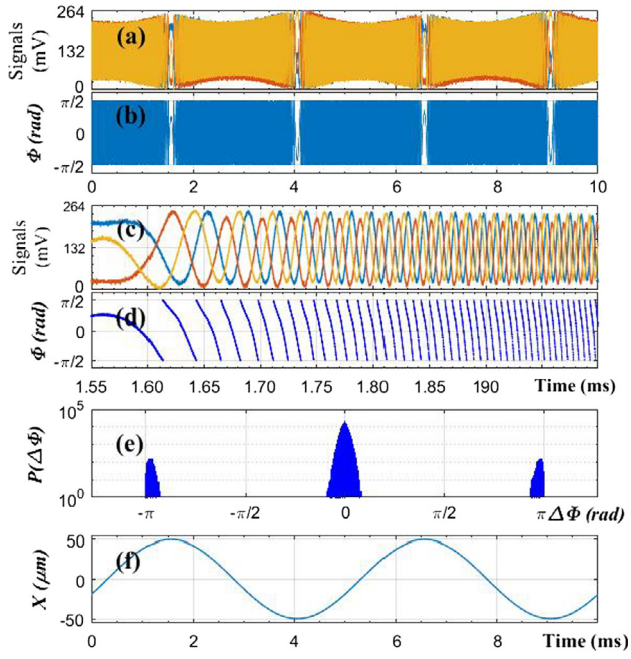

Fig. 13. Measurement of a loudspeaker motion vibrating with $f = 200$ Hz. (a) and (b) are respectively the signals detected and the fringe phase calculated in a time interval 0.01 s, (c) and (d) are the same parameters, but for a smaller time interval 2 ms, and (e) and (f) are phase increments population histogram and reconstructed motion, respectively. The transmission line bandwidth was 2.68 MHz by using 10 kΩ termination resistor parallel with the oscilloscope 1 MΩ input resistor. Wavelength of the probe beam was 632.8 nm.

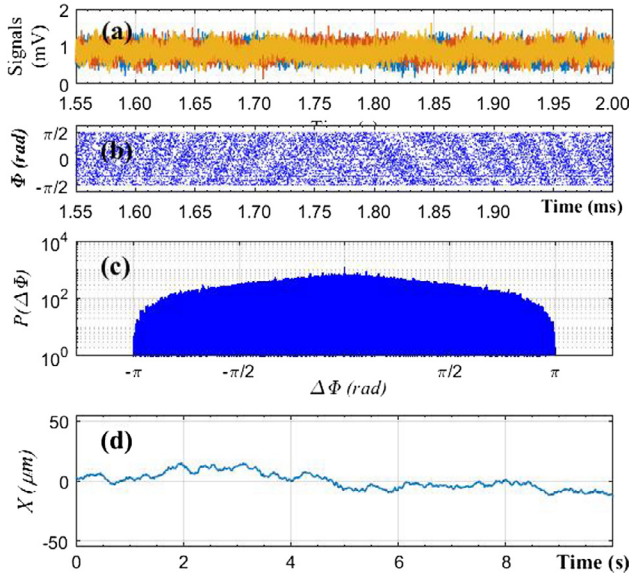

Fig. 14. Results of the same experiment of Fig. 13 with a transmission line bandwidth 0.265 GHz by using 100 Ω termination resistor.

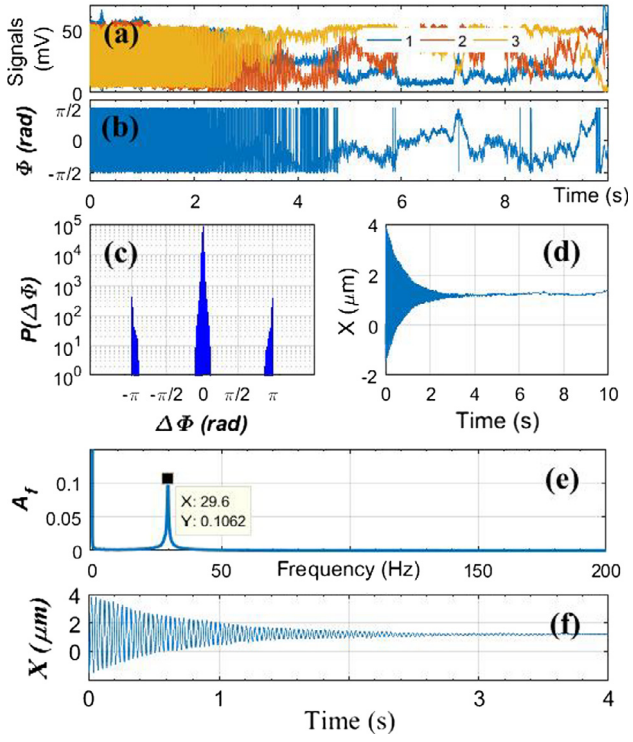

Fig. 15. Determination of the impulse response of the mounted disk, when the impulse was exerted on the middle point of the system and data acquisition rate is 50 kS/s within a 10 s time interval. (a) and (b) are respectively the signals and calculated phase, (c) is the histogram of the phase increments, (d) shows the fast Fourier transform of the motion (d), and (f) shows the motion waveform in a shorter time interval 4 s.

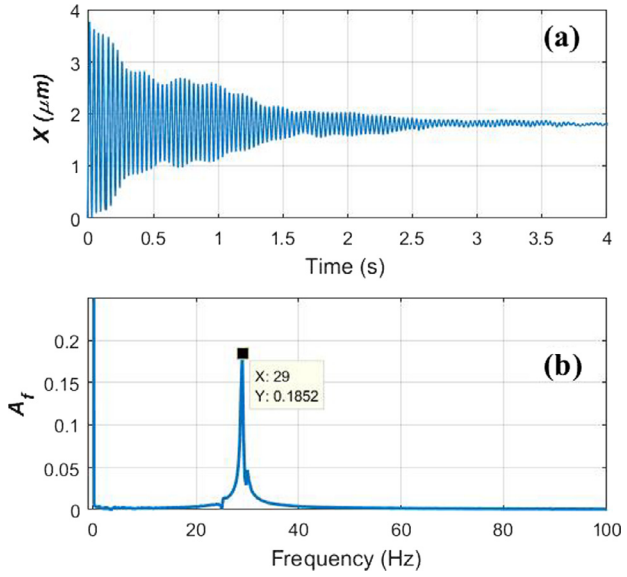

Fig. 16. Reconstructed motion or the system response (a) to an out-of-center impulse and corresponding spectrum (b). All parameters are same as the case of Fig. 15.

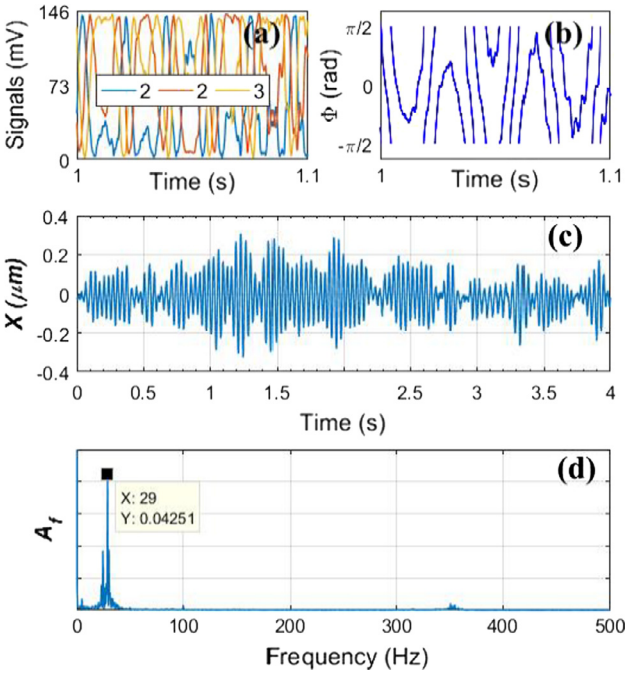

Fig. 17. Measurement on the mounted disk system in the presence of the water flow. (a) recorded signals, (b) reconstructed phase of motion for a 0.1 s time interval, (c) waveform of motion for a 4 s time interval, (d) spectrum of the motion.

calculated from the data. The system response to a non-symmetric impulse was also measured. Reconstructed motion and corresponding spectrum are shown in Fig. 16.

Results of the measurement on the disk system in the presence of the water flow are presented in Fig. 17. Recorded signals and wrapped phase of motion are illustrated respectively in (a) and (b) in a 0.1 s time interval. Waveform of the motion for a 4 s time interval is shown in (c). In (d) the spectrum of the motion is presented. On the spectrum there is a high peak at 29 Hz that corresponds to the intrinsic vibration frequency of the mounting system. The small peak around 100 Hz can be originated from the pressure fluctuation of the water pump.

8. Conclusions

Formulation, simulation, and experimentally verification of implementing a fringe chasing method based on three-point SPS for large-amplitude vibration measurements on the HoLDV was presented. By the aid of fringe chasing method, the deficiency of the HoLDV in the discrimination of the motion direction is removed. Furthermore, the effect of detectors positioning errors and finite diameter of the interfering beams were discussed and quantified. From the phase increments histogram, the adequacy of the data acquisition rate and measurement bandwidth was determined. It was shown that for typical misplacement of each of detectors equal to $\pm 0.1\Lambda$, equivalently a 0.2Λ un-equality in the inter-detectors distances, cannot lead to more than 2% PV/A distortion in the reconstructed motion. We also used the phase increments histogram as a key for the selection of the phase unwrapping tolerance value in three-point SPS method.

Acknowledgment

The authors would like to thank Mr. B. Sanaei and Mr. S. Torkamandi for their kind help on data acquisition. Also, M. H. D. thanks the INLC for their support, especially the members of thin disk laser group.

References

[1] H.-E. Albrecht, M. Borys, N. Damaschke, C. Tropea, Laser Doppler and Phase Doppler Measurement Techniques, Springer, 2002.
[2] F.J. Eberhardt, F.A. Andrews, Laser Heterodyne System for Measurement and Analysis of Vibration, J. Acoust. Soc. Am. 48 (1970) 603–609.
[3] D. Jackson, A. Kersey, M. Corke, J. Jones, Pseudoheterodyne detection scheme for optical interferometers, Electron. Lett. 18 (25) (1982) 1081–1083.
[4] J. Czarske, Chirp heterodyne laser Doppler velocimeter using a powerful fibre-coupled green laser, Optics Laser Technol. 33 (2001) 553–561.
[5] D.A. Jackson, R. Priest, A. Dandridge, A.B. Tveten, Elimination of drift in a single-mode optical fiber interferometer using a piezoelectrically stretched coiled fiber, Appl. Optics 19 (17) (1980) 2926–2929.
[6] D.O. Hogenboom, C.A. DiMarzio, Quadrature detection of a Doppler signal, Appl. Optics 37 (13) (1998) 2569–2572.
[7] T. Požar, P. Gregorčič, J. Možina, A precise and wide-dynamic-range displacement-measuring homodyne quadrature laser interferometer, Appl. Phys. B 105 (2011) 575–582.
[8] S. Rerucha, Z. Buchta, M. Sarbort, J. Lazar, O. Cip, Detection of interference phase by digital computation of quadrature signals in homodyne laser interferometry, Sensors 12 (2012) 14095–14112.
[9] D. Wu, R.-H. Zhu, L. Chen, J.-Y. Li, Transverse spatial phase-shifting method used in vibration-compensated interferometer, Optik 115 (8) (2004) 343–346.
[10] K. Weir, W.J.O. Boyle, B.T. Meggitt, A.W. Palmer, K.T.V. Grattan, A Novel adaptation of the michelson interferometer for the measurement of vibration, J. Lightwave Technol. 10 (5) (1992) 700–703.
[11] B. Hussain, M. Ahmed, G. Hussain, M. Saleem, M. Nawaz, Analog processing based vibration measurement technique using michelson interferometer, Photon. Sens. 3 (2) (2013) 137–143.
[12] S. Nakadate, M. Isshiki, Real-time vibration measurement by a spatial phase-shifting technique with a tilted holographic interferogram, Appl. Optics 36 (1) (1997) 281–284.
[13] G.B. Arfken, H.J. Weber, Mathematical Methods for Physicists, sixth ed., Elsevier Academic Press, Burlington, MA 01803, 2005.
[14] R.J. Dewhurst, Q. Shan, Optical remote measurement of ultrasound, Meas. Sci. Technol. 10 (11) (1999) R139–R168.
[15] D. Malacara, M. Servín, Z. Malacara, Interferogram Analysis for Optical Testing, CRC Press, 2005.
[16] P. Carré, Installation et Utilisation du Comparateur Photoelectrique et Interferentiel du bureau International des Poids et Measures, Metrologia 2 (1966) 13–23.
[17] D. Shmilovitz, On the definition of total harmonic distortion and its effect on measurement interpretation, IEEE Trans. Power Deliv. 20 (1) (2005) 526–528.
[18] Thorlabs, DET10A(/M) Si Biased Detector User Guide <http://www.thorlabs.com> (accessed 30 05 2017).